Revision 1

Lead–tellurium oxysalts from Otto Mountain near Baker, California: X. Bairdite, $Pb_2Cu^{2+}_4Te^{6+}_2O_{10}(OH)_2(SO_4)(H_2O)$, a new mineral with thick HCP layers.

Anthony R. Kampf[1,*], Stuart J. Mills[2], Robert M. Housley[3], George R. Rossman[3], Joseph Marty[4], and Brent Thorne[5]

[1]Mineral Sciences Department, Natural History Museum of Los Angeles County, 900 Exposition Blvd., Los Angeles, CA 90007, U.S.A.

[2]Geosciences, Museum Victoria, GPO Box 666, Melbourne 3001, Victoria, Australia

[3]Division of Geological and Planetary Sciences, California Institute of Technology, Pasadena, CA 91125, U.S.A.

[4]5199 E. Silver Oak Road, Salt Lake City, UT 84108, U.S.A.

[5]3898 S. Newport Circle, Bountiful, UT 84010, U.S.A.

*e-mail: akampf@nhm.org

ABSTRACT

Bairdite, $Pb_2Cu^{2+}_4Te^{6+}_2O_{10}(OH)_2(SO_4)(H_2O)$, is a new tellurate-sulfate from Otto Mountain near Baker, California, U.S.A. It occurs in vugs in quartz associated with khinite, cerussite, goethite, and hematite. It is interpreted as having formed from the partial oxidation of primary sulfides and tellurides during or following brecciation of quartz veins. Bairdite is monoclinic, space group $P2_1/c$, with unit cell dimensions a = 14.3126(10), b = 5.2267(3), c = 9.4878(5) Å, β =

106.815(7)°, V = 679.41(7) Å^3, and Z = 2. Bairdite occurs as diamond-shaped tabular crystals up to about 250 μm long and 5 μm thick, in subparallel and fan-shaped aggregates. The color is lime green, the streak is pale lime green, and the luster is adamantine. The Mohs hardness is estimated at between 2 and 3. Bairdite is brittle with an irregular fracture and one perfect cleavage on {100}. The calculated density based on the empirical formula is 6.062 g cm^{-3}. Bairdite is biaxial (+), with calculated indices of refraction of α = 1.953, β = 1.966, and γ = 2.039. The measured 2V is 47(2)°, dispersion is r < v, strong and the optical orientation is Y = **b**; Z ^ **a** = 34° in obtuse angle β. The pleochroism is strong: Z (pale green) <<< X (green) < Y (green). Electron microprobe analyses (average of 4) provided: PbO 34.22, CaO 0.06, CuO 23.80, TeO_3 26.34, SO_3 5.74, H_2O 2.81 (structure), total 92.97 wt%. The empirical formula (based on 17 O atoms *pfu*) is: $Pb_{2.05}Ca_{0.01}Cu^{2+}_{3.99}Te^{6+}_{2.00}S_{0.96}O_{17.00}H_{4.16}$. The eight strongest powder X-ray diffraction lines are [d_{obs} in Å (*hkl*) *I*]: 4.77 (110,-102) 50, 4.522 (002,011,-111) 66, 3.48 (multiple) 62, 2.999 (311, -411) 97, 2.701 (-502,-113,-213) 79, 2.614 (013,020) 100, 1.727 (multiple) 65, and 1.509 (-911,033,324) 83. The crystal structure of bairdite (R_1 = 0.072 for 1406 reflections with $F_o > 4\sigma F$) contains edge-sharing chains of $Te^{6+}O_6$ and $Cu^{2+}O_6$ octahedra parallel to **b** that are joined by corner-sharing in the **a** direction, forming thick stair-step-like hexagonal close packed layers parallel to {100}. The polyhedral sheet has similarities to those in the structures of timroseite and paratimroseite. The thick interlayer region contains PbO_{10} polyhedra and half-occupied SO_4 groups. Raman and infrared spectral data are presented.

Keywords: Bairdite; new mineral; tellurate; crystal structure; Raman spectroscopy, infrared spectroscopy, HCP layers; timroseite; paratimroseite; Otto Mountain, California.

INTRODUCTION

Bairdite, the new mineral described here, is the eleventh new Pb–Te oxysalt mineral (Table 1) to be described from the remarkable secondary mineral assemblage at Otto Mountain, near Baker, California, U.S.A. (Kampf et al. 2010a; Housley et al. 2011). Bairdite is named for Jerry A. Baird (born 1940) of Lake Havasu City, Arizona. Mr. Baird, a mineral collector for 45 years, has collected extensively at Otto Mountain and has provided numerous samples for research. He provided one of the two cotype specimens of bairdite and provided one of the two cotypes of the recently described mineral fuettererite (Kampf et al. 2013a). Mr. Baird has agreed to the naming of the mineral in his honor.

The new mineral and name have been approved by the Commission on New Minerals, Nomenclature and Classification of the International Mineralogical Association (IMA 2012–061). Two cotype specimens, the second collected by one of the authors (BT), are deposited in the Natural History Museum of Los Angeles County, catalogue numbers 64000 and 64001.

OCCURRENCE

Bairdite was found in the Bird Nest drift (35.27677°N, 116.09927°W) on the southwest flank of Otto Mountain, 0.4 miles northwest of the Aga mine, which is 1 mile northwest of Baker, San Bernardino County, California, U.S.A. Bairdite was also found in a quartz vein (designated NE3) northeast of the Bird Nest drift.

Bairdite is very rare and has been confirmed to occur on only four specimens, two of which were used in this study and have been designated cotypes. Bairdite crystals occur in vugs in quartz in association with khinite, cerussite, goethite, and hematite. Other minerals found elsewhere on the specimens include wulfenite and galena. Other species identified in the mineral

assemblages at Otto Mountain include acanthite, agaite, anglesite, anatacamite, atacamite, boleite, brochantite, burckhardtite, calcite, caledonite, celestine, cerussite, chalcopyrite, Br-rich chlorargyrite, chromschieffelinite, chrysocolla, devilline, diaboleite, eztlite, fluorite, fornacite, frankhawthorneite, fuettererite, gold, hessite, housleyite, iodargyrite, jarosite, khinite, kuranakhite, linarite, malachite, markcooperite, mattheddleite, mimetite, mottramite, munakataite, murdochite, muscovite, ottoite, paratimroseite, perite, phosphohedyphane, plumbojarosite, plumbotsumite, pseudoboleite, pyrite, telluroperite, thorneite, timroseite, vanadinite, and vauquelinite.

Bairdite and most of the other secondary minerals in the quartz veins are interpreted as having formed from the partial oxidation of primary sulfides (e.g. galena and chalcopyrite) and tellurides (e.g. hessite) during or following brecciation of the quartz veins. Additional background on the occurrence is provided in Kampf et al. (2010a) and Housley et al. (2011).

PHYSICAL AND OPTICAL PROPERTIES

Bairdite occurs as diamond-shaped, tabular crystals up to about 250 μm long and 5 μm thick, in subparallel and fan-shaped aggregates (Figs. 1 and 2). Tablets are flattened on {100} and bounded by the {011} form (Fig. 3). No twinning was observed optically under crossed polars or based upon single-crystal X-ray diffraction. The color is lime green, the streak is pale lime green, and the luster is adamantine. Bairdite does not fluoresce under longwave or shortwave ultraviolet light. The Mohs hardness could not be measured, but is estimated to be between 2 and 3, based upon the behavior of crystals when broken. The new mineral is brittle with irregular fracture and one perfect cleavage on {100}. The density could not be measured because it is greater than those of available high-density liquids and there is insufficient material for physical measurement. The

calculated density based on the empirical formula and single-crystal cell is 6.062 g cm^{-3}. In cold, dilute HCl, bairdite crystals rapidly turn opaque white, and then dissolve slowly.

The indices of refraction could not be measured because of the small amount of material available and the difficulty in working with liquids of sufficiently high index of refraction using a spindle stage. We have endeavored to provide optical properties based upon a combination of measurements and calculations. Bairdite is biaxial (+), with indices of refraction $\alpha = 1.953$, $\beta = 1.966$, and $\gamma = 2.039$. These were calculated from the retardation, $\beta - \alpha = 0.013$, (measured with a Berek compensator), $2V_{meas.} = 47(2)°$ (measured directly on a spindle stage), and $n_{av} = 1.986$ (based upon the Gladstone–Dale relationship for the ideal composition; Mandarino 2007). The dispersion is strong, $r < v$. The optical orientation is: $Y = \mathbf{b}$, $Z \wedge \mathbf{a} = 34°$ in obtuse angle β. Bairdite is strongly pleochroic: *Z* (pale green) <<< *X* (green) < *Y* (green).

INFRARED AND RAMAN SPECTROSCOPY

An infrared spectrum (Fig. 4) was obtained using a Nicolet Magna 860 FTIR with a KBr beamsplitter, DTGS detector, and a Nicolet Continuμm™ infrared microscope operating with a 50 × 50 μm aperture and without the use of a polarizer. The sample was a triangular half of a diamond-shaped platelet that varied between 9.1 and 9.6 μm thick. The Raman spectrum (Fig. 5) was obtained on the same crystal using a Renishaw M-1000 spectrometer with 20 mW argon ion laser operating at 514.5 nm. The spot was about 1 μm in diameter with about 5 mW at the sample when using a 100× objective lens at 100% laser power.

Prominent features visually apparent in the infrared spectrum are a set of broad bands at about 3356, 3117, 2638, 2351, 2021, 1723, and 1613 cm^{-1}. Sharper features occur at 1208 cm^{-1} (medium), strong overlapping features at about 1281 and 1060 cm^{-1}, weaker features at 973 and

116 896 cm^{-1}, a stronger band at 716 cm^{-1}, and probably features near 681 and 666 cm^{-1}, where noise
117 begins to dominate the spectrum. The absorption features in the 2400 to 3117 cm^{-1} region (and
118 possibly specifically the 2638 cm^{-1} band) arise from OH stretching from either OH or H_2O. The
119 broad band at 1613 cm^{-1} is attributable to the H_2O bending modes. The band at 716 cm^{-1} is
120 assigned to TeO_6 and that at 1060 cm^{-1} is assigned to SO_4.

121 The Raman spectrum is dominated by a feature at 721 cm^{-1}, with other significant features
122 at 977, 634, 558, 518, 378, 336, 238, and 208 cm^{-1}. With the exceptions of the 977 cm^{-1} sulfate
123 and 721 cm^{-1} tellurate features, there are comparatively few overlaps between the dominant IR
124 and Raman features in the wavenumber region where the traces coincide. Other features in the
125 Raman spectrum have not been definitely assigned, but it is likely that the 634 cm^{-1} feature is
126 from sulfate and the features between 300 and 400 cm^{-1} are from tellurate.
127

128 ## CHEMICAL COMPOSITION

129 Quantitative chemical analyses (4) of bairdite were performed using a JEOL JXA-8200
130 electron microprobe at the Division of Geological and Planetary Sciences, California Institute of
131 Technology. Analyses were conducted in WDS mode at 20 keV and 10 nA. A 10 μm beam
132 diameter was used for the first analysis and a 1 μm beam diameter was used for three subsequent
133 analyses. Crystals of bairdite proved very difficult to polish because of their fragile nature and
134 perfect cleavage. The smaller beam diameter was used because flat areas on the sample were
135 limited and generally very small. The sample was analyzed for As, Bi, Ca, Cu, Fe, P, Pb, S, Sb,
136 Si, Te, V, and Zn, but only Ca, Cu, Pb, S, and Te were above the detection limits. The standards
137 used were: anorthite (for Ca), cuprite (for Cu), galena (for Pb and S), and Sb_2Te_3 (for Te). Also,
138 no other elements were detected in EDS analyses. Analytical results are given in Table 2. There

was insufficient material for CHN analyses, so H_2O was calculated on the basis of 2 Te, charge balance and 17 total O atoms *pfu*, as determined by the crystal structure analysis (see below). Infrared spectroscopy (see above) confirmed the presence of OH and H_2O and the absence of CO_3. Note that bairdite is prone to electron beam damage, which contributes to the low analytical total. This is a common feature observed in most secondary tellurate species (e.g. Kampf et al. 2010a–f; Kampf et al. 2012; Kampf et al. 2013a,b; Mills et al. 2009, 2010).

The empirical formula (based on 17 O atoms *pfu*) is: $Pb_{2.05}Ca_{0.01}Cu^{2+}_{3.99}Te^{6+}_{2.00}S_{0.96}O_{17.00}H_{4.16}$. The simplified formula is $Pb_2Cu^{2+}_4Te^{6+}_2O_{10}(OH)_2(SO_4)(H_2O)$, which requires PbO 36.24, CuO 25.83, TeO_3 28.51, SO_3 6.50, H_2O 2.92, total 100 wt%.

X-RAY CRYSTALLOGRAPHY AND STRUCTURE DETERMINATION

All powder and single-crystal X-ray diffraction data were obtained on a Rigaku R-Axis Rapid II curved imaging plate microdiffractometer utilizing monochromatized Mo*K*α radiation. Observed powder *d*-values (with standard deviations) and intensities were derived by profile fitting using JADE 2010 software. Data (in Å) are given in Table 3. Unit cell parameters refined from the powder data using JADE 2010 with whole-pattern fitting are: a = 14.354(11), b = 5.223(11), c = 9.503(11) Å, β = 107.04(2)°, and V = 681.2(1.7) Å^3. The observed powder data fit well with those calculated from the structure, also using JADE 2010. The relatively low precision of the cell refined from the powder data is attributable to the use of Mo*K*α radiation.

The Rigaku CrystalClear software package was used for processing of the diffraction data, including the application of an empirical multi-scan absorption correction using ABSCOR

(Higashi 2001). The structure was solved by direct methods using SHELXS-97 software and was refined using SHELXL-97 (Sheldrick, 2008).

The S site refined to approximately half occupancy and three of the four O sites (O8, O9 and O10) associated with the SO_4 group also refined to roughly half occupancy, while the fourth (O7) refined to full occupancy. In the final refinement these sites were assigned half and full occupancies, accordingly, and isotropic displacement parameters were used for the O8, O9, and O10 sites. The occupancies of these sites are consistent with one SO_4 group *pfu*, as is also indicated by the empirical formula. The full occupancy of the O7 site is consistent with it participating in the SO_4 group half of the time and being an H_2O half of the time, providing one H_2O *pfu*. It is also significant that O7 forms a long bond (2.46 Å) to Cu1, while O8, O9 and O10 bond to Pb and do not participate in either Cu or Te octahedra. The bond-valence sums (BVS) for O7 as half sulfate oxygen and half water oxygen support these assignments, although the BVS when it participates in the SO_4 group is rather high (2.36 *vu*). Because the complexities of the partial occupancies make a comprehensive assignment of hydrogen bonds from O7 acting as an H_2O problematic, we did not include those hydrogen bond contributions in our bond-valence analysis. The BVS for O4 (1.31 *vu*) is indicative of it being an OH group, although this value is somewhat high for an OH. The BVS for O2 (1.59 *vu*) is quite low for an O atom; however, the short distance between O4 and O2 (2.58 Å) is indicative of a strong hydrogen bond, which serves to balance the BVS for O4 and O2.

In the difference Fourier map, significant residual electron density (17.65 e A^{-3}) was noted, centered 1.04 Å from the Pb site. This was best modeled as two separate satellite Pb peaks (PbA and PbB), which together with the main Pb peak have a total refined occupancy of almost exactly 1 Pb. The significance of these sites is not clear as their distances from the nearest O

atoms are too short for Pb–O bonds and they do not appear to represent the $6s^2$ lone electron pair of the Pb^{2+}. Note that, because of the widely dispersed remaining residual electron density, it was not possible to locate the H atoms associated with the OH and H_2O groups.

Details concerning data collection and structure refinement are provided in Table 4. Fractional coordinates and atom displacement parameters are provided in Table 5, selected interatomic distances in Table 6 and bond valences in Table 7.

DESCRIPTION OF THE STRUCTURE

In the structure of bairdite (Figure 6), individual TeO_6 octahedra and pairs of edge-sharing Jahn-Teller distorted CuO_6 octahedra link by edge-sharing into chains along *b* (Fig. 7). The chains are linked to one another by corner-sharing to form stair-step-like layers parallel to {100}. The same corner-sharing joins two such layers into a thick double layer. The region between the double layers contains half-occupied SO_4 tetrahedra and Pb^{2+}. The Pb^{2+} bonds to seven fully occupied O sites and six approximately half occupied O sites, yielding an effective coordination of ten (Figure 8). The Pb^{2+}–O bonds cover a fairly broad range (2.46 to 3.42 Å); however, there is not a pronounced lopsided distribution of bond lengths typical of Pb^{2+} with stereoactive $6s^2$ lone-pair electrons.

The same types of chains forming stair-step-like layers are found in the structures of timroseite and paratimroseite (Kampf et al. 2010b). The layer in bairdite is parallel to {100}, while those in timroseite and paratimroseite are parallel to {001}. As a consequence, the three minerals have two similar cell dimensions, those corresponding to the dimensions in these planes: for bairdite $b = 5.2257$ and $c = 9.4848$, for timroseite $a = 5.2000$ and $b = 9.6225$ Å, and for paratimroseite $a = 5.1943$ and $b = 9.6198$ Å. In the structures of timroseite and paratimroseite, the

stair-step-like layers are assembled into frameworks by corner-sharing with each successive layer reversed in orientation. This arrangement for timroseite can be seen in Figure 6. It should be noted that one of the two Cu^{2+} polyhedra participating in the chain in the paratimroseite structure is a $Cu^{2+}O_5$ square pyramid, but the overall chain and layer topology is otherwise the same as in timroseite. Another difference between the structures of timroseite and paratimroseite is that in timroseite the stair-step layers are further linked to one another by an additional $Cu^{2+}O_5$ square pyramid.

An interesting feature of the stair-step-like layers in the structures of bairdite, timroseite and paratimroseite is that they are based upon hexagonal close packing (HCP), not only in terms of the individual steps (or chains), but even with respect to the continuous assembly of steps. In the timroseite and paratimroseite structures, the HCP nature is flipped in successive layers as described above, so it does not extend over the entire framework. In the structure of bairdite, the entire thick double layer exhibits HCP and successive layers are in the same orientation, so the structure can be described as a stacking of stepped HCP layers interrupted by thick interlayer regions containing PbO_{10} polyhedra and SO_4 groups.

ACKNOWLEDGEMENTS

The paper benefited from comments by reviewer Mark Cooper and Associate Editor Fernando Colombo. The Caltech EMP analyses were supported by a grant from the Northern California Mineralogical Association and the Caltech spectroscopic work by NSF grant EAR-0947956. The remainder of this study was funded by the John Jago Trelawney Endowment to the Mineral Sciences Department of the Natural History Museum of Los Angeles County.

REFERENCES

Brown, I.D. and Altermatt, D. (1985) Bond-valence parameters from a systematic analysis of the inorganic crystal structure database. Acta Crystallographica, B41, 244–247.

Higashi, T. (2001) *ABSCOR*. Rigaku Corporation, Tokyo, Japan.

Housley, R.M., Kampf, A.R., Mills, S.J., Marty, J., and Thorne, B. (2011) The remarkable occurrence of rare secondary tellurium minerals at Otto Mountain near Baker, California – including seven new species. Rocks and Minerals, 86, 132–142.

Kampf, A.R., Housley, R.M., Mills, S.J., Marty, J. and Thorne, B. (2010a) Lead–tellurium oxysalts from Otto Mountain near Baker, California: I. Ottoite, Pb_2TeO_5, a new mineral with chains of tellurate octahedra. American Mineralogist, 95, 1329–1336.

Kampf, A.R., Marty, J. and Thorne, B. (2010b) Lead–tellurium oxysalts from Otto Mountain near Baker, California: II. Housleyite, $Pb_6CuTe_4TeO_{18}(OH)_2$, a new mineral with Cu–Te octahedral sheets. American Mineralogist, 95, 1337–1342.

Kampf, A.R., Housley, R.M. and Marty, J. (2010c) Lead–tellurium oxysalts from Otto Mountain near Baker, California: III. Thorneite, $Pb_6(Te_2O_{10})(CO_3)Cl_2(H_2O)$, the first mineral with edge-sharing octahedral dimers. American Mineralogist, 95, 1548–1553.

Kampf, A.R., Mills, S.J., Housley, R.M., Marty, J. and Thorne, B. (2010d) Lead–tellurium oxysalts from Otto Mountain near Baker, California: IV. Markcooperite, $Pb_2(UO_2)Te^{6+}O_6$, the first natural uranyl tellurate. American Mineralogist, 95, 1554–1559.

Kampf, A.R., Mills, S.J., Housley, R M., Marty, J. and Thorne, B. (2010e) Lead–tellurium oxysalts from Otto Mountain near Baker, California: V. Timroseite, $Pb_2Cu^{2+}{}_5(Te^{6+}O_6)_2(OH)_2$, and paratimroseite, $Pb_2Cu^{2+}{}_4(Te^{6+}O_6)_2(H_2O)_2$, new minerals with edge-sharing Cu–Te octahedral chains. American Mineralogist, 95, 1560–1568.

Kampf, A.R., Mills, S.J., Housley, R.M., Marty, J. and Thorne, B. (2010f) Lead–tellurium oxysalts from Otto Mountain near Baker, California: VI. Telluroperite, $Pb_3Te^{4+}O_4Cl_2$, the Te analogue of perite and nadorite. American Mineralogist, 95, 1569–1573.

Kampf, A.R., Mills, S.J., Housley, R.M., Rumsey, M.S., and Spratt, J. (2012) Lead–tellurium oxysalts from Otto Mountain near Baker, California: VII. Chromschieffelinite, $Pb_{10}Te_6O_{20}(CrO_4)(H_2O)_5$, the chromate analogue of schieffelinite. American Mineralogist, 97, 212–219.

Kampf, A.R., Mills, S.J., Housley, R.M., and Marty, J. (2013a) Lead–tellurium oxysalts from Otto Mountain near Baker, California: VIII. Fuettererite, $Pb_3Cu^{2+}{}_6Te^{6+}O_6(OH)_7Cl_5$, a new mineral with double spangolite–type sheets. American Mineralogist, 97, xxx–xxx.

Kampf, A.R., Mills, S.J., Housley, R.M., and Marty, J. (2013b) Lead-tellurium oxysalts from Otto Mountain near Baker, California: IX. Agaite, $Pb_3Cu^{2+}Te^{6+}O_5(OH)_2(CO_3)$, a new mineral with CuO_5–TeO_6 polyhedral sheets. American Mineralogist, 97, xxx–xxx.

Krivovichev, S. V. and Brown, I. D. (2001) Are the compressive effects of encapsulation an artifact of the bond valence parameters? Zeitschrift für Kristallographie, 216, 245–247.

Mandarino, J.A. (2007) The Gladstone–Dale compatibility of minerals and its use in selecting mineral species for further study. Canadian Mineralogist, 45, 1307–1324.

Mills, S.J., Kampf, A.R., Kolitsch, U., Housley, R.M., and Raudsepp, M. (2010) The crystal chemistry and crystal structure of kuksite, $Pb_3Zn_3Te^{6+}P_2O_{14}$, and a note on the crystal structure of yafsoanite, $(Ca,Pb)_3Zn(TeO_6)_2$. American Mineralogist, 95, 933–938.

Mills, S.J., Kolitsch, U., Miyawaki, R., Groat, L.A., and Poirier, G. (2009) Joëlbruggerite, $Pb_3Zn_3(Sb^{5+},Te^{6+})As_2O_{13}(OH,O)$, the Sb^{5+} analogue of dugganite, from the Black Pine mine, Montana. American Mineralogist, 94, 1012–1017.

276 Sheldrick, G.M. (2008) A short history of *SHELX*. Acta Crystallographica, A64, 112–122.

277

FIGURE CAPTIONS

Figure 1. Crystals of bairdite on quartz on cotype specimen NHMLAC 64000, FOV 1.5 mm. (Jerry Baird image; color online).

Figure 2. Bairdite crystal used in the morphological and optical studies (100 μm across; plane polarized light; color online).

Figure 3. Crystal drawing of bairdite (clinographic projection).

Figure 4. Transmission infrared spectrum through the (100) face of a crystal of bairdite.

Figure 5. Raman spectrum obtained from the (100) face of a crystal of bairdite.

Figure 6. The structures of bairdite and timroseite. Pb atoms are dark gray (blue online), SO_4 tetrahedra are very dark gray (red online), TeO_6 octahedra are light gray (yellow online), CuO_6 octahedra are gray (green online) and 5-coordinate Cu atoms and corresponding bonds (for timroseite) are gray (green online).

Figure 7. Stair-step-like layer of edge-sharing TeO_6 and CuO_6 octahedra, linked via shared corners in the structure of bairdite. Note that there are three stair-steps, increasing in elevation from left to right.

Figure 8. Pb coordination in bairdite showing Pb–O bond lengths in Å.

295 Table 1. New minerals described from Otto Mountain.

Mineral	Ideal Formula	Reference
Ottoite	$Pb_2Te^{6+}O_5$	Kampf et al. (2010a)
Housleyite	$Pb_6Cu^{2+}Te^{6+}{}_4O_{18}(OH)_2$	Kampf et al. (2010b)
Thorneite	$Pb_6(Te^{6+}{}_2O_{10})(CO_3)Cl_2(H_2O)$	Kampf et al. (2010c)
Markcooperite	$Pb_2(UO_2)Te^{4+}O_6$	Kampf et al. (2010d)
Timroseite	$Pb_2Cu^{2+}{}_5(Te^{6+}O_6)_2(OH)_2$	Kampf et al. (2010e)
Paratimroseite	$Pb_2Cu^{2+}{}_4(Te^{6+}O_6)_2(H_2O)_2$	Kampf et al. (2010e)
Telluroperite	$Pb_3Te^{4+}O_4Cl_2$	Kampf et al. (2010f)
Chromschieffelinite	$Pb_{10}Te^{6+}{}_6O_{20}(CrO_4)(H_2O)_5$	Kampf et al. (2012)
Fuettererite	$Pb_3Cu^{2+}{}_6Te^{6+}O_6(OH)_7Cl_5$	Kampf et al. (2013a)
Agaite	$Pb_3Cu^{2+}Te^{6+}O_5(OH)_2(CO_3)$	Kampf et al. (2013b)
Bairdite	$Pb_2Cu^{2+}{}_4Te^{6+}{}_2O_{10}(OH)_2(SO_4)(H_2O)$	This study

296

297

298 Table 2. Chemical analytical data for bairdite.

Constituent	Average	Range	SD	Normalized wt%
PbO	34.22	32.59–35.59	1.37	36.81
CaO	0.06	0.03–0.09	0.03	0.06
CuO	23.80	23.64–23.96	0.15	25.60
TeO_3	26.34	25.88–26.69	0.35	28.33
SO_3	5.74	5.38–5.98	0.27	6.17
H_2O*	2.81			3.02
Total	92.97			99.99†

299 * Based on the crystal structure (2 Te, charge balance and 17 O *apfu*).
300 † Rounding error.

301

Table 3. X-ray powder diffraction data for bairdite.

I_{obs}	d_{obs}	d_{calc}	I_{calc}	$h\ k\ l$	I_{obs}	d_{obs}	d_{calc}	I_{calc}	$h\ k\ l$
18	13.9(4)	13.7007	19	1 0 0			2.2650	5	2 1 3
34	6.90(4)	6.8503	75	2 0 0	26	2.196(132)	2.2078	11	5 1 1
50	4.77(9)	4.8834	9	1 1 0			2.1866	5	-5 1 3
		4.7393	20	-1 0 2			2.1582	5	-2 1 4
		4.5411	12	0 0 2	19	2.150(14)	2.1568	9	-3 2 2
66	4.522(13)	4.5301	10	0 1 1			2.1423	12	1 0 4
		4.4989	57	-1 1 1			2.0777	10	4 2 0
15	4.13(18)	4.1272	9	1 1 1	17	2.072(33)	2.0665	6	-5 0 4
21	3.98(10)	3.9803	18	1 0 2			2.0636	7	2 2 2
17	3.85(4)	3.8196	24	-3 0 2			2.0606	5	3 1 3
		3.5503	7	2 1 1	32	2.025(46)	2.0288	16	-4 2 2
62	3.48(5)	3.4768	22	-3 1 1			1.9849	6	-6 1 3
		3.4280	5	0 1 2	10	1.966(55)	1.9572	6	7 0 0
		3.4252	24	4 0 0			1.9522	7	4 2 1
14	3.35(3)	3.3633	38	2 0 2			1.8993	11	-7 1 1
39	3.241(15)	3.2185	50	-4 0 2	29	1.879(19)	1.8844	8	-5 2 2
97	2.999(9)	3.0066	100	3 1 1			1.8674	12	4 1 3
		2.9441	36	-4 1 1	3	1.831(11)	1.8378	5	6 0 2
		2.8648	5	4 1 0			1.8327	11	3 0 4
		2.8359	8	3 0 2	2	1.783(12)	1.7831	5	-2 1 5
		2.7198	20	-5 0 2			1.7384	16	-6 2 2
79	2.701(5)	2.7008	27	-1 1 3			1.7357	7	-4 1 5
		2.6810	67	-2 1 3	65	1.727(5)	1.7195	6	6 2 0
100	2.614(5)	2.6197	43	0 1 3			1.7158	9	0 1 5
		2.6134	30	0 2 0			1.7092	14	7 1 1
		2.5665	9	-3 1 3			1.7017	6	3 2 3
7	2.521(18)	2.5602	22	4 1 1			1.6936	5	5 1 3
		2.5114	8	0 2 1			1.6568	5	1 2 4
		2.4417	6	2 2 0	27	1.633(11)	1.6328	7	-8 1 3
13	2.436(10)	2.4360	6	1 2 1			1.6266	7	0 3 2
		2.4214	6	-2 2 1	39	1.600(11)	1.5972	27	-6 1 5
		2.4188	7	4 0 2			1.5798	9	-3 0 6
		2.3282	5	-6 0 2			1.5743	5	3 3 1
		2.3179	5	-3 0 4			1.5103	9	-9 1 1
34	2.282(18)	2.2834	13	6 0 0	83	1.509(4)	1.5100	11	0 3 3
		2.2790	12	-3 2 1			1.5005	7	3 2 4

Note: Only calculated lines with intensities of 5 or greater are listed.

Table 4. Data collection and structure refinement details for bairdite.

Diffractometer	Rigaku R-Axis Rapid II
X-ray radiation	Mo*K*α (λ = 0.71075 Å)
Temperature	298(2) K
Ideal formula	$Pb_2Cu^{2+}{}_4Te^{6+}{}_2O_{10}(OH)_2(SO_4)\cdot H_2O$
Space group	$P2_1/c$
Unit cell dimensions	a = 14. 3126(10) Å
	b = 5.2267(3) Å
	c = 9.4878(5) Å
	β = 106.815(7)º
Z	2
Volume	679.41(7) Å^3
Density (for above formula)	6.021 g cm^{-3}
Absorption coefficient	35.303 mm^{-1}
F(000)	1080
Crystal size	40 x 35 x 5 μm
θ range	4.17 to 27.48°
Index ranges	$-18 \le h \le 18$, $-6 \le k \le 6$, $-12 \le l \le 12$
Reflections collected/unique	15177/1554 [R_{int} = 0.113]
Reflections with $F_o > 4\sigma F$	1406
Completeness to θ = 25.01°	99.9%
Max. and min. transmission	0.8432 and 0.3325
Refinement method	Full-matrix least-squares on F^2
Parameters refined	138
GoF	1.173
Final R indices [$F_o > 4\sigma F$]	R_1 = 0.0715, wR_2 = 0.1626
R indices (all data)	R_1 = 0.0774, wR_2 = 0.1656
Extinction coefficient	0.0001(2)
Largest diff. peak/hole	+4.66/-2.38 e A^{-3}

*$R_{int} = \Sigma|F_o^2\text{-}F_o^2(\text{mean})|/\Sigma[F_o^2]$. GoF = $S = \{\Sigma[w(F_o^2-F_c^2)^2]/(n-p)\}^{1/2}$. $R_1 = \Sigma||F_o|\text{-}|F_c||/\Sigma|F_o|$. $wR_2 = \{\Sigma[w(F_o^2-F_c^2)^2]/\Sigma[w(F_o^2)^2]\}^{1/2}$. $w = 1/[\sigma^2(F_o^2) + (aP)^2 + bP]$ where a is 0.0161, b is 120.54 and P is $[2F_c^2 + \text{Max}(F_o^2,0)]/3$.

Table 5. Fractional coordinates and atomic displacement parameters for bairdite.

	occ.	*x*/*a*	*y*/*b*	*z*/*c*	U_{eq}	U_{11}	U_{22}	U_{33}	U_{23}	U_{13}	U_{12}
Pb	0.873(9)	0.34148(7)	0.0795(3)	0.39773(15)	0.0218(5)	0.0184(6)	0.0217(9)	0.0261(7)	0.0012(6)	0.0077(4)	-0.0008(4)
PbA	0.049(9)	0.3421(13)	0.965(7)	0.437(3)	0.016(8)						
PbB	0.076(7)	0.3415(11)	0.850(5)	0.4112(18)	0.033(6)						
Te	1.0	0.16195(10)	0.4933(3)	0.49077(15)	0.0156(5)	0.0155(8)	0.0209(8)	0.0114(7)	-0.0005(5)	0.0053(5)	-0.0003(5)
Cu1	1.0	0.7926(2)	0.4758(5)	0.8472(3)	0.0167(7)	0.0181(14)	0.0214(15)	0.0116(13)	-0.0001(10)	0.0059(10)	0.0001(10)
Cu2	1.0	0.9079(2)	0.5282(5)	0.1916(3)	0.0184(7)	0.0206(14)	0.0195(15)	0.0166(14)	0.0012(11)	0.0079(11)	0.0008(11)
S	0.5	0.5334(8)	0.087(3)	0.1993(13)	0.024(3)	0.013(5)	0.035(7)	0.023(6)	0.005(5)	0.003(4)	0.003(5)
O1	1.0	0.8577(12)	0.144(3)	0.8362(15)	0.019(3)	0.036(9)	0.019(8)	0.007(7)	-0.001(6)	0.012(6)	0.008(7)
O2	1.0	0.0766(12)	0.209(3)	0.4836(18)	0.023(4)	0.020(8)	0.026(9)	0.018(8)	-0.009(7)	-0.001(7)	-0.004(7)
O3	1.0	0.2700(12)	0.291(3)	0.6011(18)	0.020(3)	0.023(8)	0.016(8)	0.023(8)	0.001(7)	0.009(7)	-0.002(6)
O4	1.0	0.0453(11)	0.696(3)	0.3687(16)	0.019(3)	0.017(8)	0.024(9)	0.011(7)	-0.005(6)	0.000(6)	-0.002(6)
O5	1.0	0.1757(13)	0.156(3)	0.808(2)	0.026(4)	0.025(9)	0.026(9)	0.033(10)	0.003(8)	0.017(8)	0.003(7)
O6	1.0	0.7648(12)	0.291(3)	0.012(2)	0.024(4)	0.021(8)	0.011(8)	0.040(10)	0.004(7)	0.008(7)	0.007(6)
O7	1.0	0.6267(18)	0.091(5)	0.183(3)	0.055(7)	0.052(14)	0.077(18)	0.048(13)	0.033(13)	0.032(12)	0.023(13)
O8	0.5	0.530(3)	0.032(7)	0.354(4)	0.030(8)						
O9	0.5	0.493(3)	0.862(9)	0.115(5)	0.046(11)						
O10	0.5	0.480(3)	0.329(8)	0.142(5)	0.038(9)						

Table 6. Selected bond lengths (Å) in bairdite.

Pb–O6	2.463(16)	Cu1–O5	1.913(18)	Te–O6	1.880(16)
Pb–O8 (×½)	2.60(4)	Cu1–O6	1.979(18)	Te–O2	1.912(17)
Pb–O10 (×½)	2.62(3)	Cu1–O1	1.984(16)	Te–O1	1.915(15)
Pb–O5	2.665(18)	Cu1–O3	2.002(16)	Te–O3	1.916(16)
Pb–O3	2.671(16)	Cu1–O2	2.415(17)	Te–O5	1.958(17)
Pb–O7	2.74(3)	Cu1–O7	2.46(2)	Te–O4	2.034(16)
Pb–O3	2.785(16)	<Cu–O>	2.126	<Te–O>	1.936
Pb–O9 (×½)	2.82(4)				
Pb–O7	2.85(3)	Cu2–O1	1.945(14)	S–O7	1.39(2)
Pb–O8 (×½)	2.86(4)	Cu2–O2	1.980(16)	S–O9	1.45(5)
Pb–O10 (×½)	2.99(4)	Cu2–O4	2.002(17)	S–O10	1.50(4)
Pb–O1	3.281(17)	Cu2–O5	2.040(18)	S–O8	1.51(4)
Pb–O9 (×½)	3.42(5)	Cu2–O4	2.355(15)	<S–O>	1.46
<Pb–O>	2.811*	Cu2–O6	2.572(18)		
		<Cu–O>	2.149	Hydrogen bond	
				O4···O2	2.58(2)

* Based upon 10-coordination with bond lengths to half-occupied O atoms given 0.5 weight.

Table 7. Bond valence sums for bairdite. Values are expressed in valence units.

	O1	O2	O3	O4	O5	O6	$O7_S$	$O7_W$	O8	O9	O10	Σ
Pb	0.07		0.24 0.19		0.24	0.36	0.20 ×½ → 0.16 ×½ →	0.20 ×½ → 0.16 ×½ →	0.27 ×½ → 0.16 ×½ →	0.17 ×½ → 0.05 ×½ →	0.26 ×½ → 0.12 ×½ →	1.98
Cu1	0.44	0.14	0.42		0.53	0.44	0.12 ×½ →	0.12 ×½ →				2.09
Cu2	0.49	0.44		0.42 0.16	0.38	0.09						1.98
Te	1.01	1.01	1.00	0.73	0.90	1.11						5.76
S							1.88		1.36	1.60	1.40	6.24
H		0.26		0.74								1.00
Σ	2.01	1.85	1.85	2.05	2.05	2.00	2.36	0.48	1.79	1.82	1.78	

Notes: O7 is a sulfate oxygen half of the time (O7s) and an H_2O half of the time (O7w). Pb^{2+}–O bond strengths are from Krivovichev and Brown (2001); Te^{6+}–O, Cu^{2+}–O and S^{6+}–O bond strengths are from Brown and Altermatt (1985) as is the hydrogen bond strength for O2···O4.

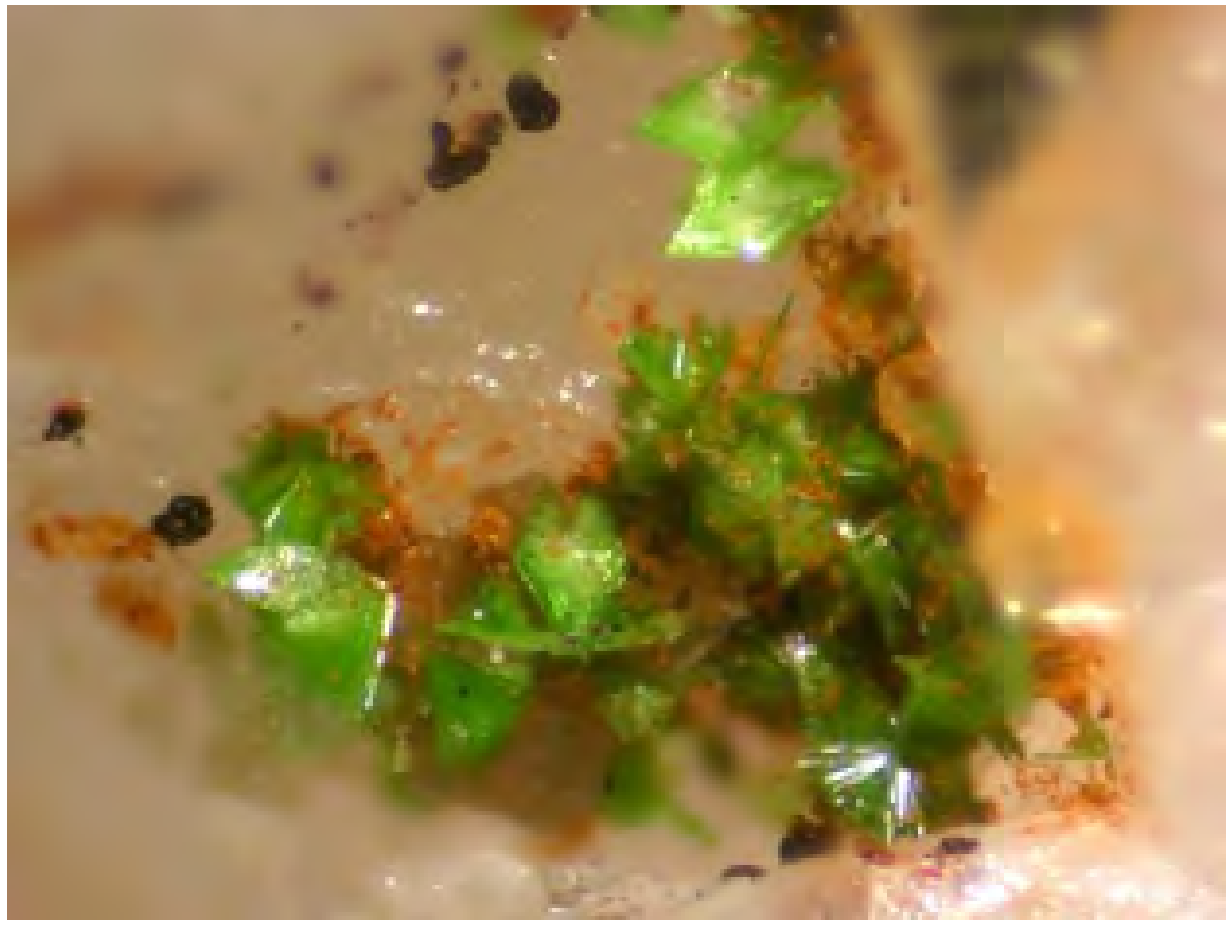

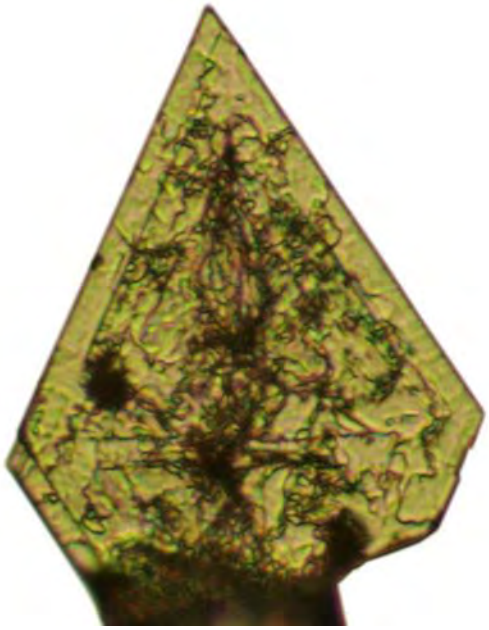

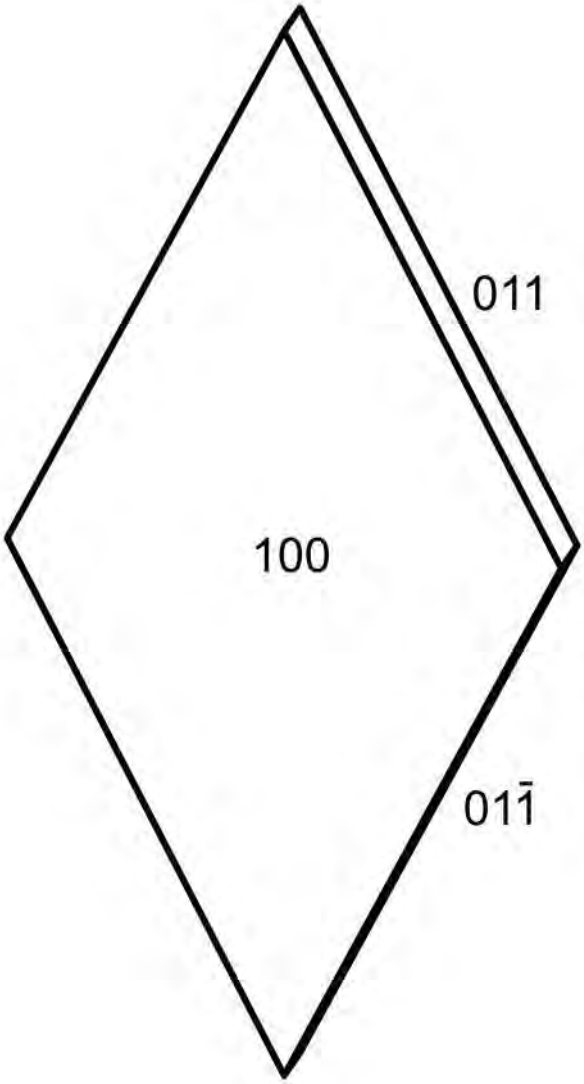
011
100
01$\bar{1}$

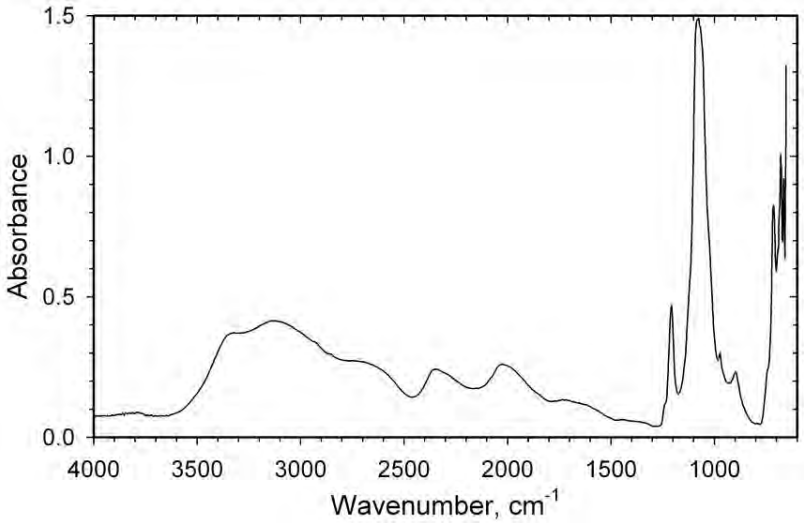
1.5
1.0
0.5
0.0
Absorbance
4000
3500
3000
2500
2000
1500
1000
Wavenumber, cm-1

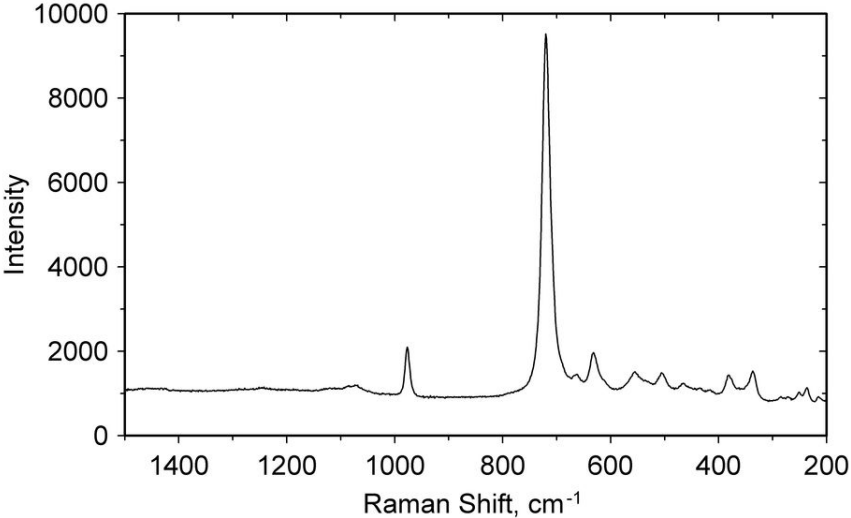
10000
8000
6000
4000
2000
0
Intensity
1400
1200
1000
800
600
400
200
Raman Shift, cm-1

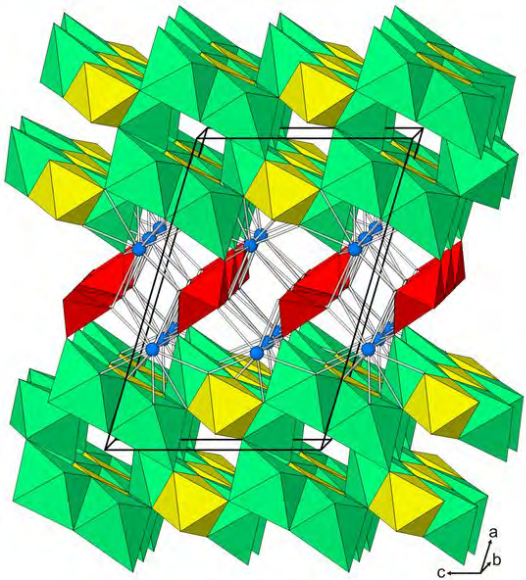

bairdite

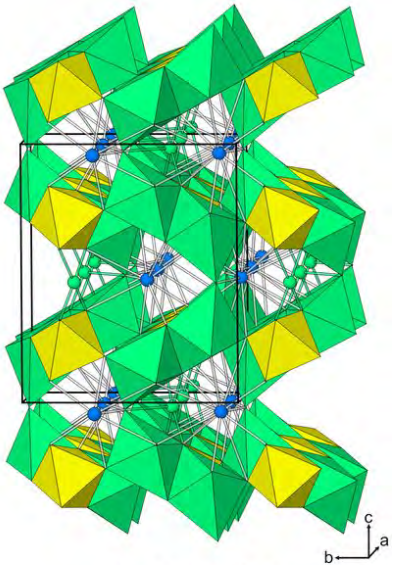

timroseite

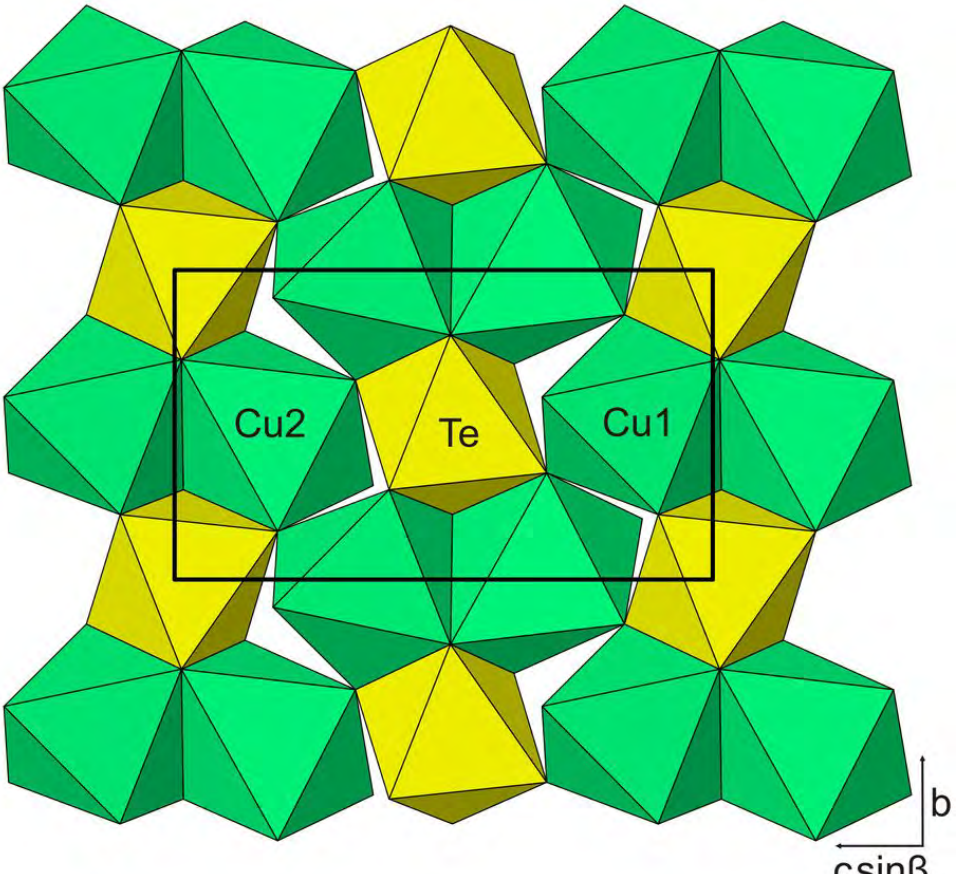
Cu2
Te
Cu1
b
csinβ

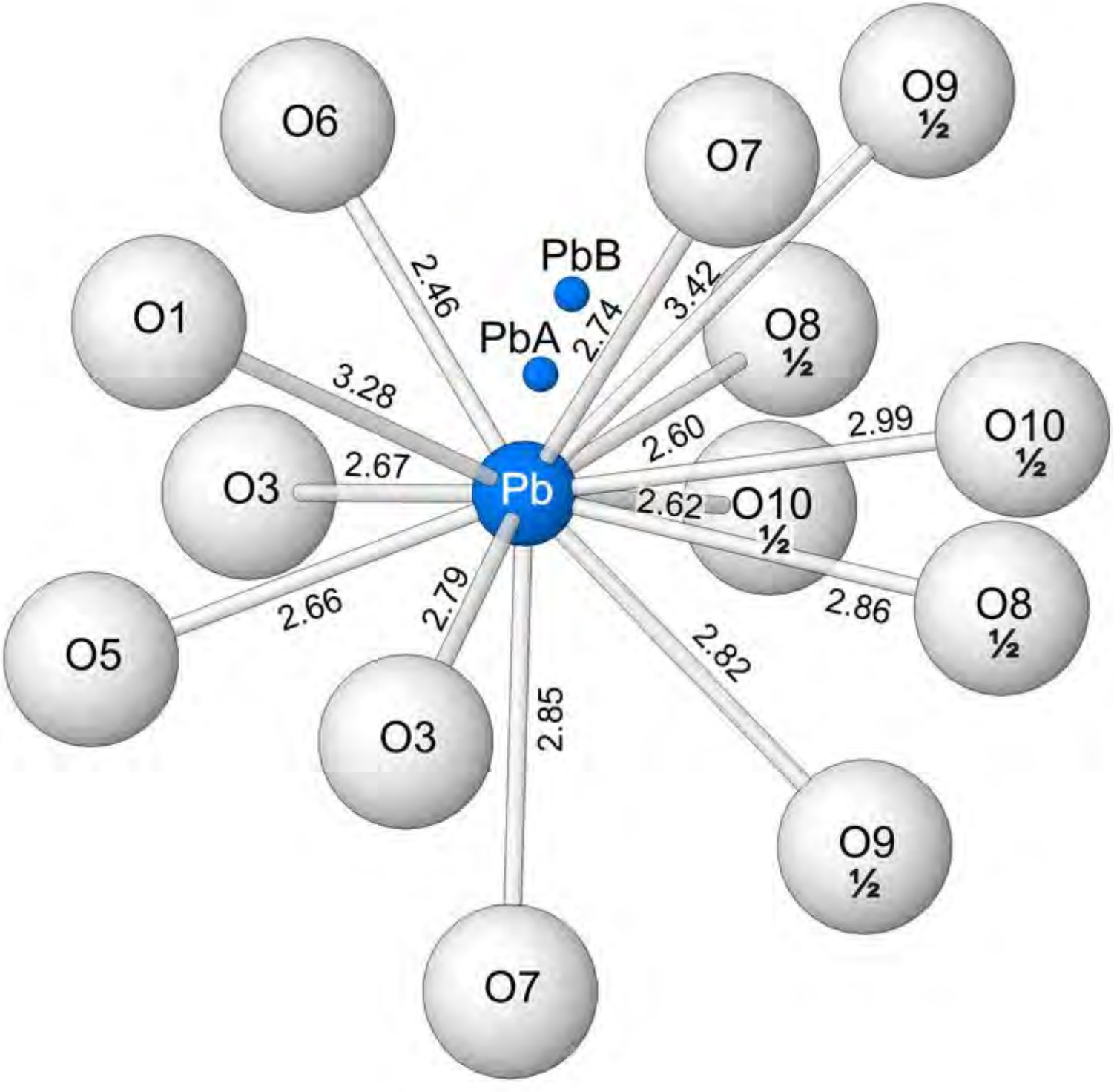
O6
O7
O9
½
PbB
PbA
2.46
2.74
3.42
O1
O8
½
3.28
2.60
2.99
O10
½
O3
2.67
Pb
2.62
O10
½
2.66
2.79
2.86
O8
½
O5
2.82
O3
2.85
O9
½
O7